This is a preprint of: "Phase portraits for some symmetric cubic Riccati polynomial differential equations", Jaume Llibre, Regilene D. S. Oliveira, Clàudia Valls, *Topology Appl.*, vol. 234, 220–237, 2018.
DOI: [10.1016/j.topol.2017.11.023]

PHASE PORTRAITS FOR $\mathbb{Z}_2$-SYMMETRIC CUBIC RICCATI POLYNOMIAL DIFFERENTIAL EQUATIONS

JAUME LLIBRE[1], REGILENE OLIVEIRA[2] AND CLÁUDIA VALLS[3]

Abstract. We classify the topological phase portraits in the Poincaré disc of all $\mathbb{Z}_2$-symmetric cubic Riccati polynomial differential systems .

1. Introduction and statement of the main results

The first works on Riccati equations appear in manuscripts of XVI–century by Count Riccati, who was mainly interested in studying the problem of separation of variables in quadratic and time-varying scalar systems, see [16]. Since then, in the subsequent centuries many contributions appeared regarding these equations. Nowadays it has been shown that Riccati differential equations appear in many applications such as in control, dynamic games, river flow, linear systems with Markovian jumps, invariant embedding, stochastic control theory, econometric models and diffusion problems (see for instance [2, 3, 4, 5, 7, 8, 9, 10, 11, 16, 17]).

A Riccati differential equation is of the form

$$\frac{dy}{dx} = A(x)y^2 + B(x)y + C(x),$$

or equivalently to the differential system

$$\begin{aligned} \dot{x} &= d(x),\\ \dot{y} &= a(x)y^2 + b(x)y + c(x), \end{aligned}$$

where $A(x) = a(x)/d(x)$, $B(x) = b(x)/d(x)$ and $C(x) = c(x)/d(x)$. In general, there is no method for solving this differential system because it is a nonhomogeneous differential system of degree two in the variable y and, therefore, a complete analysis of it does not exist. In order to understand the behavior of its solutions (without knowing explicitly them) one good approach is to characterize the phase portraits of such systems for obtaining its qualitative behavior.

Among the nonlinear systems, the quadratic are the easiest ones. Therefore there are many papers in the literature concerning quadratic systems and in particular, quadratic Riccati differential systems, see [1, 14] and the references therein. In this paper we are interested in studying the *cubic Riccati polynomial differential systems*, more precisely the global phase portraits of cubic Riccati polynomial differential systems. Note that such systems have the form

$$\begin{aligned} \dot{x} &= d_0 + d_1x + d_2x^2 + d_3x^3,\\ \dot{y} &= (a_0 + a_1x)y^2 + (b_0 + b_1x + b_2x^2)y + c_0 + c_1x + c_2x^2 + c_3x^3, \end{aligned} \tag{1}$$

2010 *Mathematics Subject Classification.* Primary 37J35, 37K10.
Key words and phrases. Riccati polynomial differential systems, vector fields, phase portrait, reversibility, equivariance.

where $a_0, a_1, b_0, b_1, b_2, c_0, c_1, c_2, c_3, d_0, d_1, d_2, d_3 \in \mathbb{R}$. We always have $a_0^2 + a_1^2 \neq 0$ (otherwise the system is not Riccati), $a_1^2 + b_2^2 + c_3^2 + d_3^2 \neq 0$ otherwise it is not cubic differential system. Note that the global phase portrait of the quadratic Riccati equation is studied in [13], so we consider the case of cubic Riccati differential system. As system (1) has 13 parameters it is unabordable so we restrict our study to the ones that are $\mathbb{Z}_2$-symmetric. It is well know that are two types of $\mathbb{Z}_2$-symmetry: reversibility and equivariance.

Without loss of generality in this paper a vector field $X : \mathbb{R}^2 \to \mathbb{R}^2$ is $\mathbb{Z}_2$- *reversible* if

$$\begin{pmatrix} -1 & 0 \\ 0 & 1 \end{pmatrix} X(x, y) = -X(-x, y)$$

and is $\mathbb{Z}_2$-*equivariant* if

$$\begin{pmatrix} -1 & 0 \\ 0 & 1 \end{pmatrix} X(x, y) = X(-x, y).$$

Vector fields with symmetry appear very often in applications so the study of symmetric vector fields is an old subject. Nowadays it has been an increasing interest in reversible and equivariant systems see [12] and the references cited there.

By definition system (1) is $\mathbb{Z}_2$-reversible and its components have no common factors if and only if it reduces to

$$\begin{aligned} \dot{x} &= d_0 + d_2 x^2, \\ \dot{y} &= x(a_1 y^2 + b_1 y + c_1 + c_3 x^2), \end{aligned} \tag{2}$$

where $d_0 a_1 c_3 \neq 0$; and it is $\mathbb{Z}_2$-equivariant if and only if it reduces to

$$\begin{aligned} \dot{x} &= d_1 x + d_3 x^3, \\ \dot{y} &= a_0 y^2 + (b_0 + b_2 x^2) y + c_0 + c_2 x^2, \end{aligned} \tag{3}$$

where $d_3^2 + b_2^2 \neq 0$ and $a_0 \neq 0$.

We say that two polynomial vector fields in the Poincaré disc are *topologically equivalent* if there exists a homeomorphism from one onto the other which sends orbits to orbits preserving or reversing the direction of the flow.

Our main result is the following one.

Theorem 1. *A $\mathbb{Z}_2$-reversible cubic Riccati polynomial differential system* (2) *after a linear change of variables and a rescaling of its independent variable can be written as*

$$\dot{x} = 1 + bx^2, \quad \dot{y} = x(y^2 + ex^2 + d), \qquad b \in \{-1, 0, 1\}, d, e \in \mathbb{R}; \tag{4}$$

Moreover the global phase portraits on the Poincaré disc of these families are topologically equivalent to the phase portraits in Figure 1

(a) (1), (2) *with* $b \in \{0, 1\}$ *and* $e = 0$,
(b) (3), (4), (5), (6) *with* $b \in \{0, 1\}$ *and* $e \neq 0$,
(c) (1), (7), (8) *with* $b = -1$ *and* $e = 0$,
(d) (3), (4), (5), (6), (9), (10), (11), (12) *with* $b = -1$ *and* $e \neq 0$.

Theorem 2. *A $\mathbb{Z}_2$-equivariance cubic Riccati polynomial differential system* (3) *after a linear change of variables and a rescaling of its independent variable can be written as one of the following six classes:*

(I) $\dot{x} = x(x^2 + a)$, $\dot{y} = c_0 + c_1 x^2 + y^2 + x^2 y$ *with* $a, c_0, c_1 \in \mathbb{R}$;

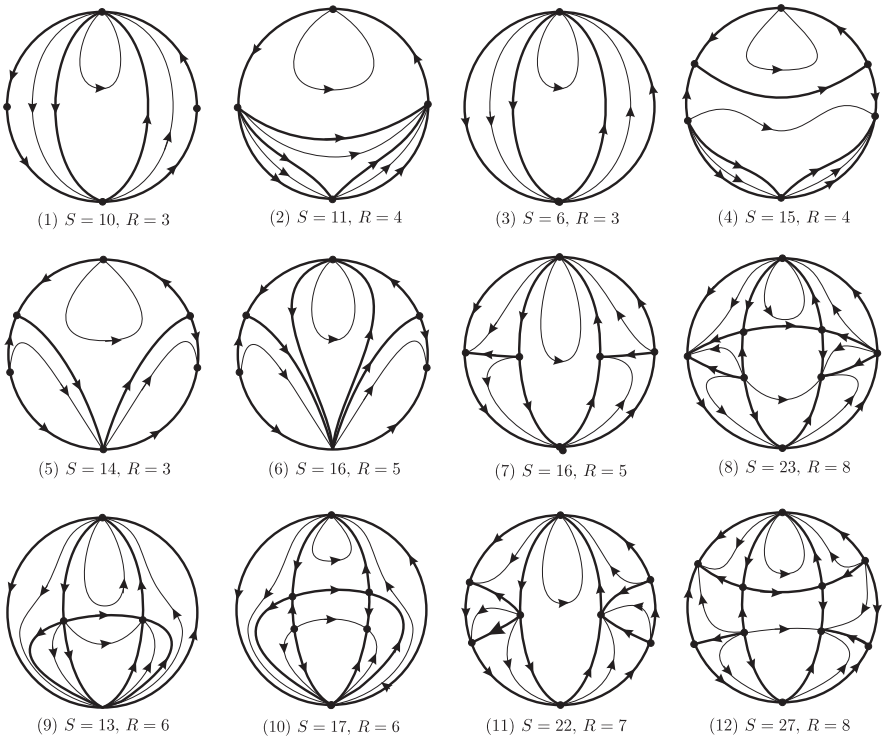

FIGURE 1. Phase portraits on the Poincaré disc of system (4): (1) $d > 0, e = 0$ and $b = -1, 0, 1$; (2) $d \leq 0$, $e = 0$ and $b = 0, 1$; (3) $e > 0$, $b = 0, 1$ or $e > 0$, $b = -1$ and $d+e > 0$; (4), (5) and (6) $e < 0$, $b = 0, 1$ or $e < 0, b = -1$ and $d+e > 0$; (7) $e = 0, b = -1$ and $d = 0$; (8) $e < 0, b = -1$ and $d < 0$; (9) $e > 0$, $d + c = 0$; (10) $e > 0$, $d + e < 0$; (11) $e < 0$, $b = -1$ and $d + e = 0$; (12) $e < 0, b = -1$ and $d + e < 0$. Here S denotes the number of separatrices and R the number of canonical regions, as in Theorem 5.

(II) $\dot{x} = x(x^2 + a),\ \dot{y} = c_0 + c_1x^2 + y^2 - x^2y$ *with* $a, c_0, c_1 \in \mathbb{R}$*;*
(III) $\dot{x} = x(x^2 + 1),\ \dot{y} = c_0 + c_1x^2 + y^2$ *with* $c_0, c_1 \in \mathbb{R}$*;*
(IV) $\dot{x} = x(x^2 - 1),\ \dot{y} = c_0 + c_1x^2 + y^2$ *with* $c_0, c_1 \in \mathbb{R}$*;*
(V) $\dot{x} = x,\ \dot{y} = c_0 + c_1x^2 + y^2 + x^2y$ *with* $c_0, c_1 \in \mathbb{R}$*;*
(VI) $\dot{x} = x,\ \dot{y} = c_0 + c_1x^2 + y^2 - x^2y$ *with* $c_0, c_1 \in \mathbb{R}$*.*

Moreover the global phase portraits on the Poincaré disc of these six families are topologically equivalent to the phase portraits

(a) (1) – (13) *of Figure 2 for system (I);*
(b) (1) – (16) *of Figure 3 for systems (II);*
(c) (1), (10), (11), (12), (13), (14), (15) *of Figure 3 for systems (III);*
(d) (1), (2), (3), (4), (5), (6), (8), (9), (17) *of Figure 3 for systems (IV);*
(e) (1) – (7) *of Figure 4 for systems (V);*
(f) (1), (10), (10), (11), (12), (13), (14), (15) *of Figure 3 for systems (VI).*

From the proof of Theorem 2 follows the next result.

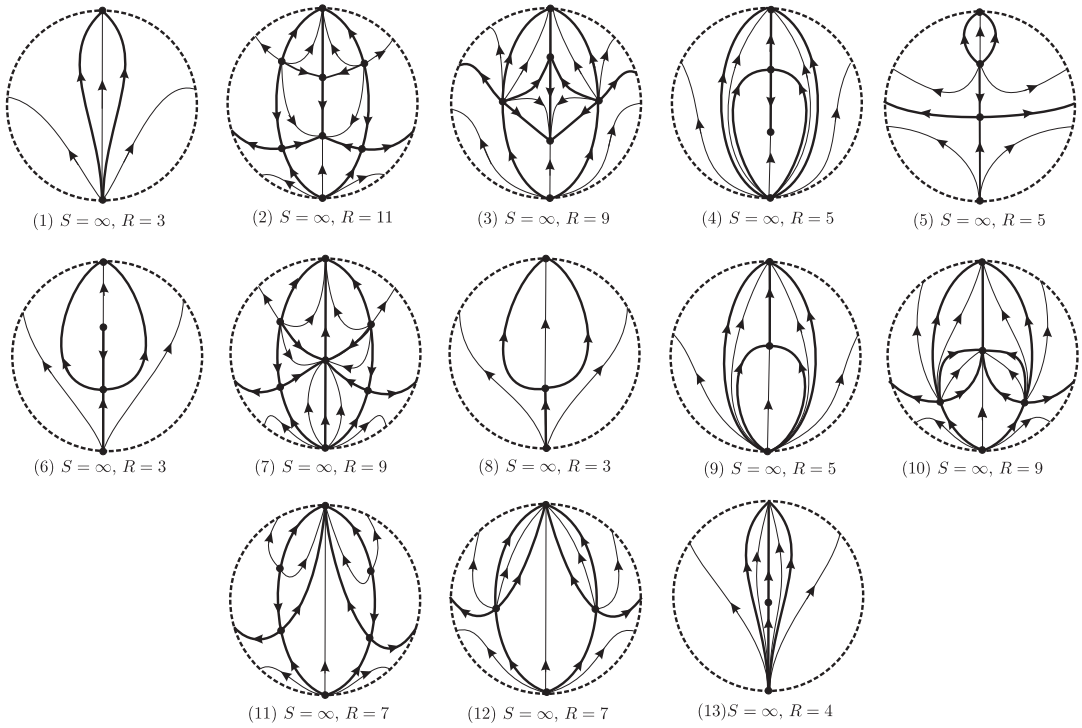

FIGURE 2. Phase portraits on the Poincar disc of system (I):(1) $c_0 > 0$ and $a \geq 0$ or $c_0 > 0, a < 0$ and $\Delta < 0$; (2)$c_0 < 0, a < 0$ and $\Delta > 0$; (3) $c_0 < 0, a < 0$ and $\Delta = 0$; (4) $c_0 < 0, a < 0$ and $\Delta < 0$; (5) $c_0 < 0$ and $a > 0$; (6) $c_0 < 0$ and $a = 0$; (7) $c_0 = 0, a < 0$ and $\Delta > 0$; (8) $c_0 = 0$ and $a > 0$ or $c_0 = a = 0$ and $c_1 \leq 0$; (9) $c_0 = 0, a < 0$ and $\Delta < 0$; (10) $c_0 = 0, a < 0$ and $\Delta = 0$; (11) $c_0 > 0, a < 0$ and $\Delta > 0$; (12) $c_0 > 0, a < 0$ and $\Delta = 0$ and (13) $c_0 = a = 0$ and $c_1 > 0$. Here S denotes the number of separatrices and R the number of canonical regions, as in Theorem 5.

Corollary 3. *The phase portraits of system (III) and system (VI) of Theorem 2 are topologically equivalent.*

In the following section we give some preliminary definitions and results on the Poincaré sphere and the Poincaré compactification. In section 3 we prove how to obtain the normal forms given in Theorem 1. In section 4 we prove Theorem 1. Theorem 2 is proved in sections 5 and 6.

2. Poincaré compactification

In this section we summarize the Poincaré compactification that we shall use for describing the global phase portraits of our Riccati systems. For more details on the Poincaré compactification see Chapter 5 of [6].

Let $\mathbb{S}^2$ be the *Poincaré sphere* $\{(s_1, s_2, s_3) \in \mathbb{R}^3 : s_1^2 + s_2^2 + s_3^2 = 1\}$. Given a polynomial vector field

$$X = (\dot{x}, \dot{y}) = (P(x, y), Q(x, y))$$

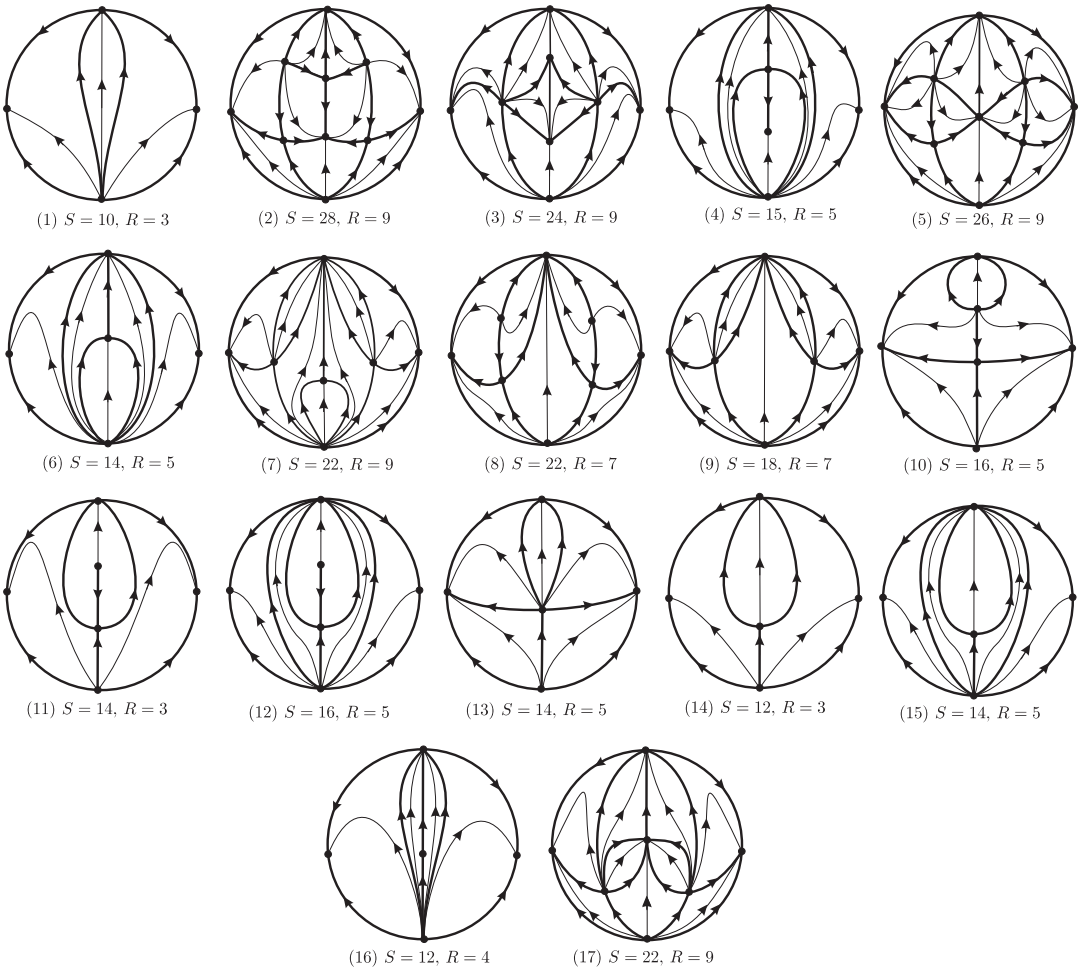

FIGURE 3. Phase portraits on the Poincaré disc of systems (II), (III), (IV) and (VI): (1) system (II) with $c_0 > 0, a < 0$ and $\Delta < 0$ or $c_0 > 0$ and $a \geq 0$, system (III) and (VI) with $c_0 > 0$ and system (IV) with $c_0 > 0$ and $\Delta < 0$; (2) system (II) with $c_0 < 0, a < 0$ and $\Delta > 0$ and system (IV) with $c_0 < 0$ and $\Delta > 0$; (3) system (II) with $c_0 < 0, a < 0$ and $\Delta = 0$ and system (IV) with $c_0 < 0$ and $\Delta = 0$; (4) system (II) with $c_0 < 0, a < 0$ and $\Delta < 0$ and system (IV) with $c_0 < 0$ and $\Delta < 0$; (5) system (II) with $c_0 = 0, a < 0$ and $\Delta > 0$ and system (IV) with $c_0 = 0$ and $\Delta > 0$; (6) system (II) with $c_0 = 0, a < 0$ and $\Delta < 0$ and system (IV) with $c_0 = 0$ and $\Delta < 0$; (7) system (II) with $c_0 = 0, a < 0$ and $\Delta = 0$; (8) system (II) with $c_0 > 0, a < 0$ and $\Delta > 0$ and system (IV) with $c_0 > 0$ and $\Delta > 0$; (9) system (II) with $c_0 > 0, a < 0$ and $\Delta = 0$ and system (IV) with $c_0 > 0$ and $\Delta = 0$; (10) system (II) with $c_0 < 0$ and $a > 0$, system (III) and (VI) with $c_0 < 0$; (11) system (II) with $c_0 < 0$ and $a > 0$, system (III) and (VI) with $c_0 < 0$; (12) system (II) with $c_0 < 0$ and $a > 0$, system (III) and (VI) with $c_0 < 0$; (13) system (II) with $c_0 = 0$ and $a > 0$ or $c_0 = a = 0$ and $c_1 \leq 0$, system (III) and (VI) with $c_0 = 0$; (14) system (II) with $c_0 = 0$ and $a > 0$, system (III) and (VI) with $c_0 = 0$; (15) system (II) with $c_0 = 0$ and $a > 0$, system (III) and (VI) with $c_0 = 0$; (16) system (II) with $c_0 = a = 0$ and $c_1 > 0$; (17) system (IV) with $c_0 = 0$ and $c_1 = 0$.

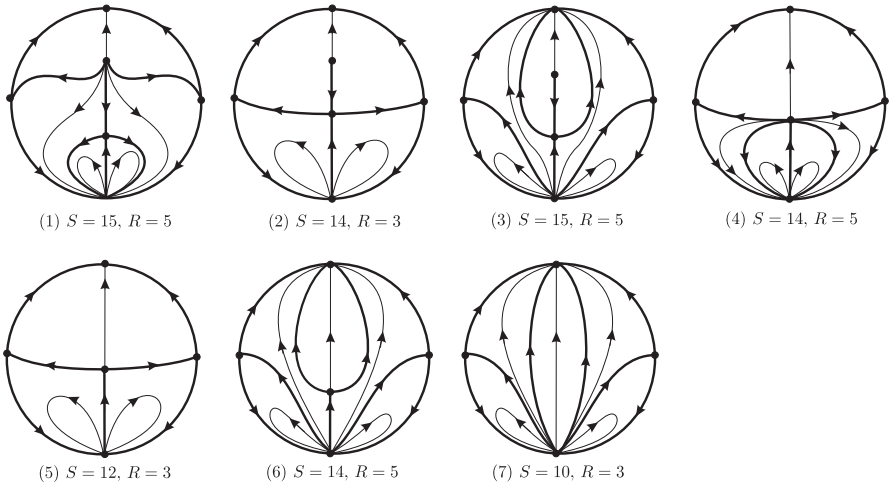

FIGURE 4. Global phase portraits on the Poincaré disc of system (V): (1), (2) and (3) for $c_0 < 0$; (4) for $c_0 = 0$ and (5), (6) and (7) for $c_0 > 0$. Here S denotes the number of separatrices and R the number of canonical regions of each phase portrait.

in $\mathbb{R}^2$ we extend it to the Poincaré sphere by sending each point $x \in \mathbb{R}^2$ identified wiht the point $(x_1, x_2, 1) \in \mathbb{R}^3$ to the Poincaré sphere $\mathbb{S}^2$ using the straight line through the origin of $\mathbb{R}^3$ and x. In this way we get two copies of X: one on the northern hemisphere $\{(s_1, s_2, s_3) \in \mathbb{S}^2 : s_3 > 0\}$ and another on the southern one $\{(s_1, s_2, s_3) \in \mathbb{S}^2 : s_3 < 0\}$. Clearly the equator $\mathbb{S}^1 = \{(s_1, s_2, s_3) \in \mathbb{S}^2 : s_3 = 0\}$ can be identified with the infinity of $\mathbb{R}^2$. For studying the Poincaré sphere we use the local charts

$$U_i = \{\mathbf{s} \in \mathbb{S}^2 : s_i > 0\}, \quad V_i = \{\mathbf{s} \in \mathbb{S}^2 : s_i < 0\},$$

where $\mathbf{s} = (s_1, s_2, s_3)$, with the local maps

$$\phi_i(s) : U_i \to \mathbb{R}^2, \quad \psi_i(s) : V_i \to \mathbb{R}^2,$$

defined by $\phi_i(s) = -\psi_i(s) = \left(\dfrac{s_m}{s_i}, \dfrac{s_n}{s_i}\right)$ for $m < n$ and $m, n \neq i$, for $i = 1, 2, 3$. The expression of the extended vector field $p(X)$ on $\mathbb{S}^2$ is

$$\dot{u} = v^d \left[-uP\left(\frac{1}{v}, \frac{u}{v}\right) + Q\left(\frac{1}{v}, \frac{u}{v}\right)\right], \quad \dot{v} = -v^{d+1} P\left(\frac{1}{v}, \frac{u}{v}\right); \tag{5}$$

in the local chart U_1,

$$\dot{u} = v^d \left[P\left(\frac{u}{v}, \frac{1}{v}\right) - uQ\left(\frac{u}{v}, \frac{1}{v}\right)\right], \quad \dot{v} = -v^{d+1} Q\left(\frac{u}{v}, \frac{1}{v}\right); \tag{6}$$

in the local chart U_2, and

$$\dot{u} = P(u, v), \quad \dot{v} = Q(u, v), \tag{7}$$

in the local chart U_3, where d is the degree of the polynomial vector field X. The expressions of the extended vector field in the charts V_i are the same than for the charts U_i multiplied by $(-1)^{d-1}$, for $i = 1, 2, 3$. In short, to study the vector field X, it is sufficient to study its

Poincaré compactification $p(X)$ restricted to the northern hemisphere plus $\mathbb{S}^1$. To draw the phase portraits, we consider the projection by $\pi(s_1, s_2, s_3) = (s_1, s_2)$ of the closed northern hemisphere to the plane $s_3 = 0$. The image of this projection is called the Poincaré disc $\mathcal{D}$.

The singular points of this compactification which are in the interior of $\mathcal{D}$ are the *finite singular points* of X. The singular points of the vector field on the boundary $\mathbb{S}^1$ the Poincaré disc are the *infinite singular points* of X. If $s \in \mathbb{S}^1$ is an infinite singular point, then $-s \in \mathbb{S}^1$ is also an infinite singular point, and the local phase portrait of one is that of the other multiplied by $(-1)^{d-1}$. Note that to study the infinite singular points it is enough to study the infinite singular points at $U_1|_{v=0}$ and at the origin of U_2.

Neumann [15] characterizes when two vector fields in the Poincaré disc $\mathcal{D}$ are topologically equivalent. Two polynomial vector fields $\mathcal{X}$ and $\mathcal{Y}$ on $\mathbb{R}^2$ are *topologically equivalent* if there exists a homeomorphism on $\mathcal{D}$ preserving the infinity $\mathbb{S}^1$ carrying orbits of the flow induced by $p(\mathcal{X})$ into orbits of the flow induced by $p(\mathcal{Y})$ preserving or reversing the orientation of the all orbits.

Let $\mathcal{D}$ be the Poincaré disc and $p(\mathcal{X})$ be the Poincaré compactification on $\mathcal{D}$ of a polynomial differential system defined in $\mathbb{R}^2$. Consider ϕ the analytic flow associated to $p(\mathcal{X})$ and denote by (U, ϕ) the flow of ϕ on an invariant set $U \subset \mathcal{D}$. The flow (U, ϕ) is *parallel* if it is topologically equivalent to one to the following flows:

(i) the flow in $\mathbb{R}^2$ given by the differential system $\dot{x} = 1, \dot{y} = 0$, known as *strip flow*.

(ii) the flow in $\mathbb{R}^2 \setminus \{0\}$ given in polar coordinates by the differential system $\dot{r} = 0$, $\dot{\theta} = 1$, known as *annular flow*;

(iii) the flow in $\mathbb{R}^2 \setminus \{0\}$ given in polar coordinates by the differential system $\dot{r} = r$, $\dot{\theta} = 0$, known as *spiral or radial flow*.

The separatrices of a polynomial vector field $p(\mathcal{X})$ in the Poincaré disc $\mathcal{D}$ are the orbits of $p(\mathcal{X})$ on the boundary of the Poincaré disc, all finite singular points of $p(\mathcal{X})$, all limit cycles of $p(\mathcal{X})$, and all separatrices of the hyperbolic sectors of the finite and infinite singular points of $p(\mathcal{X})$.

Denote by $\mathbb{S}$ the union of the separatrices of $(\mathcal{D}, \phi)$ defined by $p(\mathcal{X})$. $\mathbb{S}$ is an invariant closed set. In addition, if N is a connected component of $\mathcal{D} \setminus \mathbb{S}$, then N is an invariant set under the flow ϕ. For a given vector field $p(\mathcal{X})$ its *separatrix configuration* is formed by all the separatrices of $p(\mathcal{X})$ plus an orbit in each one of its canonical regions.

The next two results are fundamental in the description of the phase portrait of a flow associated to the planar polynomial vector field $p(\mathcal{X})$.

Theorem 4. *Suppose that the number of separatrices of the flow $(\mathcal{D}, \phi)$ is finite. Then every canonical region of the flow $(\mathcal{D}, \phi)$ is parallel.*

Theorem 5. *Let $(\mathcal{D}, \phi)$ and $(\mathcal{D}, \psi)$ be two compactified Poincaré flows with finitely many separatrices. Then they are topologically equivalent if and only if their separatrix configurations are topologically equivalent.*

The proofs of Theorems 4 and 5 can be found in [15]. From Theorem 5 it follows that to classify the phase portrait in the Poincaré disc of a planar polynomial differential system having finitely many triceratopes it is enough to describe their separatrix configuration.

Definition 1. *A differential system*

$$\dot{x} = P(x, y), \qquad \dot{y} = Q(x, y), \tag{8}$$

has a contact point (x_0, y_0) *with the straight line* $ax + by + c = 0$ *if* $aP(x_0, y_0) + bQ(x_0, y_0) = 0$.

The next result will be useful in the study of the global phase portrait of system (1).

Lemma 6. *A cubic polynomial differential system* (8) *has either at most three contact points with a straight line* L *or* L *is invariant straight line by the cubic system.*

Proof. Let $L = ax + by + c = 0$ be a straight line which is not an invariant line of the system. Then a contact point (x_0, y_0) between L and an orbit of the system is a solutions of

$$aP(x_0, y_0) + bQ(x_0, y_0) = 0. \tag{9}$$

Assume $a \neq 0$ (otherwise replacing a by b in the argument the proof is analogous). Then $L = 0$ becomes $x_0 = (-c - by_0)/a$. Introducing x_0 in (9) we get a cubic polynomial in the variable y which has at most three solutions. This concludes the proof. □

3. Obtaining the normal forms given in Theorems 1 and 2

Proposition 7. *A* $\mathbb{Z}_2$*-reversible cubic Riccati polynomial differential system* (2) *after a linear change of variables and a rescaling of its independent variable, can be written as* (4).

Proof. Doing a linear change of variables and a rescaling of the independent variable (the time) of the form $x \to \alpha X, y \to \beta Y + \delta, t \to \gamma T$, with $\beta\delta\gamma \neq 0$, system (2) becomes

$$\begin{aligned}
\dot{X} &= \frac{d_0\alpha}{\gamma} + \frac{d_2\alpha^3}{\gamma}X^2,\\
\dot{Y} &= X\Big(\frac{\alpha\beta}{\gamma}(c_1 + b_1\delta + a_1\delta^2) + \frac{\alpha\beta^2}{\gamma}Y(b_1 + 2a_1\delta) + \frac{\alpha^3\beta}{\gamma}c_3X^2 + \frac{\alpha\beta^3}{\gamma}a_1Y^2\Big).
\end{aligned}$$

Since $d_0a_1 \neq 0$ we take $\gamma = d_0\alpha$, $\beta = (d_0/a_1)^{1/3}$, $\delta = -b_1/2a_1$ and

$$\alpha = \begin{cases} 1 & \text{if } d_2 = 0,\\ (d_2/d_0)^{1/2} & \text{if } d_2d_0 > 0,\\ (-d_2/d_0)^{1/2} & \text{if } d_2d_0 < 0. \end{cases}$$

Renaming the variables we obtain the systems (4). □

Proposition 8. *A* $\mathbb{Z}_2$*-equivariant cubic Riccati polynomial differential system* (3) *after a linear change of variables and a rescaling of its independent variable can be written as one of the six classes (I) - (V) given in Theorem 2.*

Proof. Doing a linear change of variables and a rescaling of the independent variable (the time) of the form $x \to \alpha X, \quad y \to \beta Y + \delta, \quad t \to \gamma T$, with $\beta\delta\gamma \neq 0$, system (3) becomes

$$\begin{aligned}
\dot{X} =& \frac{d_1\alpha^2}{\gamma}X + \frac{d_3\alpha^4}{\gamma}X^3,\\
\dot{Y} =& \frac{\beta}{\gamma}(c_0 + b_0\delta + a_0\delta^2) + \frac{\beta^2}{\gamma}Y(b_0 + 2a_0\delta) + \frac{\alpha^2\beta}{\gamma}X^2(c_2 + b_2\delta)\\
&+ \frac{\beta^3}{\gamma}a_0Y^2 + \frac{\alpha^2\beta^2}{\gamma}b_2X^2Y.
\end{aligned} \tag{10}$$

Since $a_0 \neq 0$ we take $\beta = (\gamma/a_0)^{1/3}$. Now we consider three different cases.

If $d_3 b_2 \neq 0$ we take $\gamma = d_3\alpha^4$, $\delta = -b_0/(2a_0)$ and

$$\alpha = \begin{cases} a_0/b_2(d_3/b_2)^{1/2} & \text{if } d_3 b_2 > 0, \\ a_0/b_2(-d_3/b_2)^{1/2} & \text{if } d_3 b_2 < 0. \end{cases}$$

Renaming the variables we get systems (I) and (II) of Theorem 2.

If $d_3 \neq 0$ and $b_2 = 0$ we take $\gamma = d_3\alpha^4$, $\delta = -b_0/(2a_0)$ and

$$\alpha = \begin{cases} (d_1/d_3)^{1/2} & \text{if } d_1 d_3 > 0, \\ (-d_1/d_3)^{1/2} & \text{if } d_1 d_3 < 0. \end{cases}$$

Renaming the variables we obtain systems (III) and (IV) of Theorem 2.

If $d_3 = 0$ then $d_1 b_2 \neq 0$. In this case we take $\gamma = d_1\alpha^2$, $\delta = -b_0/(2a_0)$ and

$$\alpha = \begin{cases} (a_0^2 d_1/b_2^3)^{1/4} & \text{if } d_1 b_2 > 0 > 0, \\ (-a_0^2 d_1/b_2^3)^{1/4} & \text{if } d_1 b_2 < 0. \end{cases}$$

Renaming the variables we get systems (V) and (VI) of Theorem 2. This completes the proof. □

4. Global behavior of systems (4) of Theorem 1

To study the singular points at infinity of a polynomial vector field via the Poincaré compactification we need to study the singular points in the local chart U_1 and the origin of the local chart U_2.

The Poincaré compactification $p(\mathcal{X})$ of system (4) in the local chart U_1 is given by

$$\begin{aligned} \dot{u} &= e + u^2 - buv + dv^2 - uv^3, \\ \dot{v} &= -bv^2 - v^4. \end{aligned}$$

If $e > 0$ there are no singular points in the local chart U_1. If $e = 0$ the unique singular point in this chart is the origin. If $e < 0$, $(u, v) = (\pm\sqrt{-e}, 0)$ are the unique singular points in the local chart U_1. In this last case, using Theorem 2.19 of [6] we get that both points are saddle-nodes.

When $e = 0$ the origin is identically zero and so we apply blowing ups to study it. Applying the blow up $(u, v) \to (u, w)$, where $u = u$ and $w = v/u$ and a rescaling $ds = udt$ we get the following system

$$\begin{aligned} \dot{u} &= -u(-1 + bw - dw^2 + u^2 w^3) \\ \dot{w} &= -w(1 + dw^2). \end{aligned}$$

This system has the origin as a singular point which is a hyperbolic saddle. If $d \geq 0$ there are no more singular points. If $d < 0$ there are two more singular points: $(0, \pm 1/\sqrt{-d})$. If $b \neq 0$ these points have eigenvalues $\mp b/\sqrt{-d}$, 2, and so one is a saddle and the other is an unstable node. If $b = 0$ then we have that both singular points are semi-hyperbolic. Using Theorem 2.19 in [6] we obtain that the point $(0, 1/\sqrt{-d})$ is a semi-hyperbolic saddle and the point $(0, -1/\sqrt{-d})$ is a a semi-hyperbolic node.

From the blow down we get the local behavior shown in Figures 5 and 6 for the solutions in a neighborhood of the origin of the local chart U_1. In Figure 5 the blowing down on the left hand side corresponds to the case $e = 0$, $b = -1, 0, 1$ and $d > 0$; the blowing down on the right hand

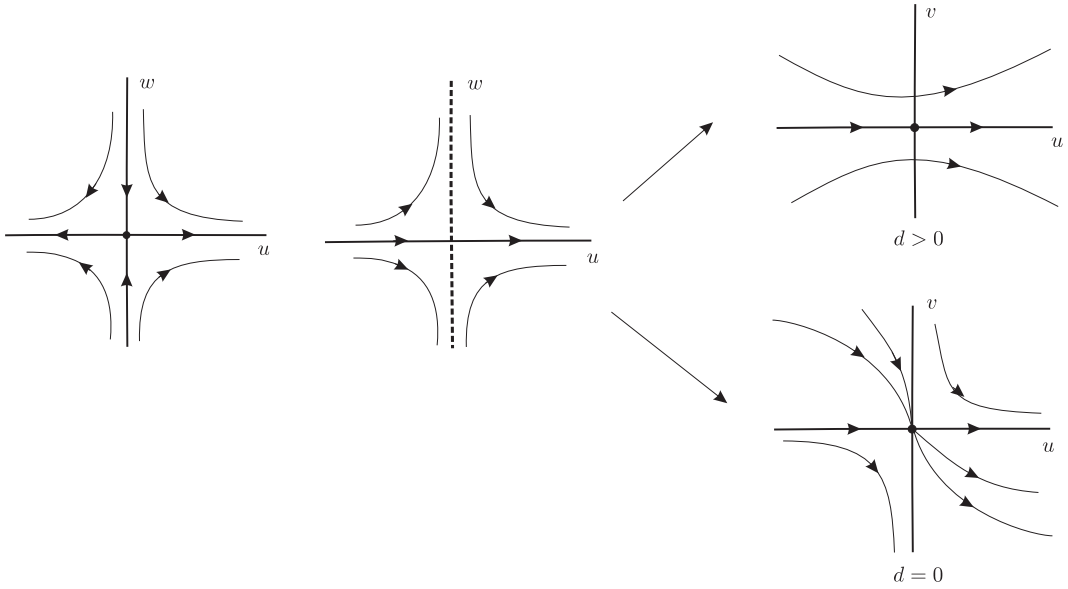

FIGURE 5. Blowing down of the origin of the local chart U_1 for $e = 0$, $b = -1, 0, 1$ and $d > 0$ on the top; and for $e = 0$, $b = -1, 0, 1$ and $d = 0$ on the botton.

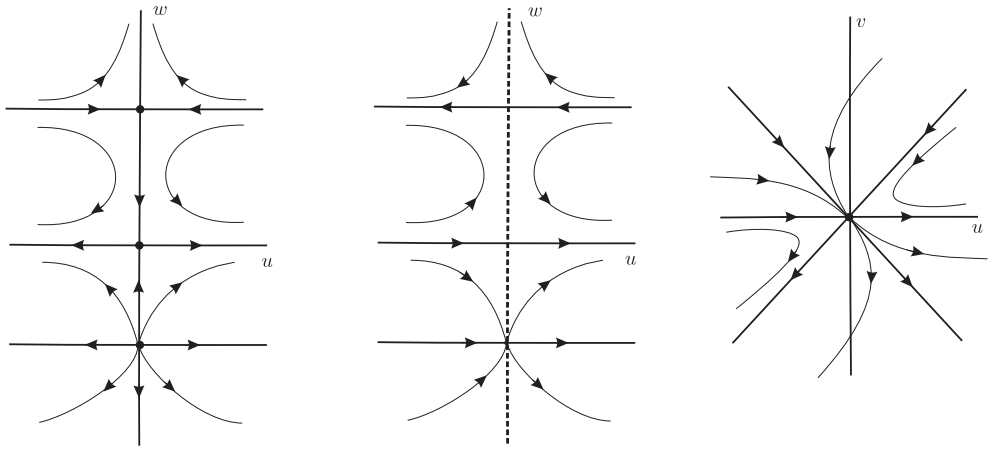

FIGURE 6. Blowing down of the origion of the local chart U_1 for $e = 0$, $b = -1, 0, 1$ and $d < 0$.

side corresponds to the case $e = 0$, $b = -1, 0, 1$ and $d = 0$. In Figure 6 is the blowing downs which corresponds to the case when $e = 0$, $b = -1$ and $d < 0$.

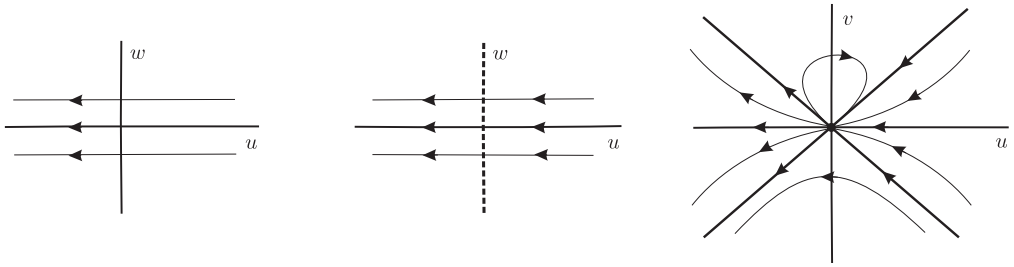

FIGURE 7. Blowing down of the origin of the local chart U_2 of system (4).

System (4) in the local chart U_2 is written as

$$\begin{aligned}\dot{u} &= -u^2 + bu^2v + v^3 - eu^4 - du^2v^2,\\ \dot{v} &= -uv(1 + eu^2 + dv^2),\end{aligned}$$

having the origin as a linearly zero equilibrium point.

Applying the blow up $(u, v) \to (u, w)$, where $u = u$ and $w = v/u$ and the rescaling $ds = u^2dt$ we get the following system

$$\begin{aligned}\dot{u} &= -1 - eu^2 + buw - du^2w^2 + uw^3,\\ \dot{w} &= -w^2(b + w^2),\end{aligned}$$

which has no singular points when $u = 0$. From the blow down we get the local behavior shown in Figure 7 for the solutions in a neighborhood of the origin in the local chart U_2.

If $b = 0, 1$ or $b = -1$ and $d > -e$ there are no finite singular points in systems (4). If $b = -1$ and $d < -e$ there are four singular points $P^1_\pm = (1, \pm\sqrt{-d-e})$ with eigenvalues -2 and $\mp 2\sqrt{-d-e}$ and $P^2_\pm = (-1, \pm\sqrt{-d-e})$ with eigenvalues 2 and $\mp 2\sqrt{-d-e}$. So P^1_+ and P^2_+ are saddles, P^1_- is an unstable node and P^2_- is a stable node. Finally, when $d = -e$ systems (4) has only two singular points $(\pm 1, 0)$ which are semi-hyperbolic. Using Theorem 2.19 in [6] we conclude that they both are saddle-nodes.

We remark that if $b = -1$ system (4) has two invariant straight lines $x = \pm 1$ and if $e = 0$ and $d < 0$ system (4) has additionally two invariant straight lines $y = \pm\sqrt{-d}$. Due to the $\mathbb{Z}_2$-reversibility we can restrict the study of the global phase portrait to $x > 0$ (with the opposite orientation when $x < 0$).

4.1. **Global phase portraits for systems** (4) **with** $b = 0, 1$ **and** $e = 0$**.** As studied previously there are no finite singular points and the local behavior in the local charts in the infinite are describe in Figures 5, 6 and 7. Taking into account that when $d < 0$ system (4) has the two invariant straight lines $y = \pm\sqrt{-d}$, that coalesces when $d = 0$, and disappear when $d > 0$ we get the global phase portrait (1) of Figure 1 when $d > 0$ and (2) of Figure 1 when $d \leq 0$.

4.2. **Global phase portraits for systems** (4) **with** $b = 0, 1$ **and** $e \neq 0$**.** In this case there are no finite singular points and the local behavior in the local chart U_2 is given in Figure 7. When $e > 0$ there are no singular points in the local chart U_1. So the global phase portrait is (3) of Figure 1. When $e < 0$ the separatrizes of the saddle-nodes in the local chart U_1 determine the

three possible configurations (4), (5) and (6) of Figure 1, depending on their ω and α–limits. Choosing $d = 3$, $e = -1$ we get the global phase portrait (4) of Figure 1, and choosing $d = 3$, $e = -0.01$ we get (6) of Figure 1. By continuity (5) also holds (it corresponds to a separatrix connextion).

4.3. **Global phase portraits for systems** (4) **with** $b = -1$ **and** $e = 0$**.** In this case $b = -1$ and we have two invariant straight lines $x = \pm 1$. The sign of the parameter d determines the finite behavior as well as the existence of other invariant straight lines. More precisely, if $d < 0$ there are two more invariant straight lines $y = \pm\sqrt{-d}$ and the singular points are on the intersection of the invariant straight lines. This fact together with the local behavior at infinty studied before, imply that the unique global phase portrait is (8) of Figure 1. If $d = 0$, there is a third invariant straight line which is $y = 0$ and the singular points coalesced. So, we get the phase portrait (7) of Figure 1. Finally if $d > 0$ there are neither finite singular points nor additional invariant straight lines and the global phase portrait is (1) of Figure 1.

4.4. **Global phase portraits for systems** (4) **with** $b = -1$ **and** $e \neq 0$**.** .

In this case there are two invariant straight lines $x = \pm 1$. The sign of e determines the local behavior in the local chart U_1 and the sign of $-d - e$ determines the finite behavior. We recall that due to the symmetry we can restrict to study $x \geq 0$.

If $e > 0$, as before there are no singular points in the local chart U_1 so we have a different global phase portrait in the Poincaré disc depending on whether $-d - e < 0$, $-d - e = 0$, or $-d - e > 0$. In each case the finite behavior determines completely the global phase portraits, which are (3), (9) and (10) of Figure 1, respectively.

If $e < 0$ and $-d - e < 0$ due to the study done before and repeating arguments as the case $e = 0$, we get the global phase portraits (4), (5) and (6) of Figure 1.

Finally, if $e < 0$ and $-d - e > 0$ there are four finite singular points $(\pm 1, \pm\sqrt{-d-e})$. Note that the point $(1, \sqrt{-d-e})$ is a saddle and that on the local chart U_1 we have two saddle nodes $(\pm\sqrt{-e}, 0)$. Moreover, according to the orientation of the flow, the possible α-limit of the separatrix of the saddle $(1, -\sqrt{-d-e})$ are: the origin of the local chart V_2 and $(\pm\sqrt{-e}, 0)$ on the local chart U_1. Note that

$$\dot{y}|_{y=-\sqrt{-d-e}} < 0 \quad \text{and that } \sqrt{-e} > -\sqrt{-d-e}.$$

Hence, the α–limit of the separatrix of $(1, -\sqrt{-d-e})$ must be $(-\sqrt{-e}, 0)$ of the local chart U_1 and by continuity we get that the unique possible topological equivalent global phase portrait is (12) of Figure 1.

If $e < 0$ and $d = -e$ the finite saddle and the unstable node on the invariant line $x = 1$ coalesce. So, taking into account that in the case $-d - e > 0$ there is a unique possible global phase portrait, we conclude that the unique possible global phase portrait under these conditions is (11) of Figure 1.

5. Global behavior of systems (I)–(IV) of Theorem 2

In this section we study the local behavior of systems (I) to (IV) of Theorem 2. Note that systems (I)- (IV) can be written as the following unique system

$$\begin{aligned} \dot{x} =& x^3 + ax, \\ \dot{y} =& c_0 + c_1 x^2 + y^2 + f x^2 y, \end{aligned} \tag{11}$$

with $f \in \{-1, 0, 1\}$ and $a, c_0, c_1 \in \mathbb{R}$ and that when $f = 0$, then $a \in \{-1, 1\}$.

We recall that to study the singuar points at infinity of a polynomial vector field via the Poincaré compactification we need to study the singular points in the local chart U_1 and the origin of the local chart U_2. The Poincaré $p(X)$ of system (11) in the local chart U_1 is given by

$$\begin{aligned} \dot{u} =& (f-1)u + c_1 v + u^2 v - auv^2 + c_0 v^3, \\ \dot{v} =& -v - av^3. \end{aligned}$$

If $f = 1$ the curve $v = 0$ is filled with singular points and after the rescaling $ds = vdt$, the curve $v = 0$ is no longer invariant. If $f \neq 1$ the unique singular point in the local chart U_1 is the origin with eigenvalues -1 and $-1 + f$, and since $f \in \{-1, 0\}$ we get that this point is a stable node.

System (11) in the local chart U_2 is written as

$$\begin{aligned} \dot{u} =& -uv + (1-f)u^3 + auv^2 - c_1 u^3 v - c_0 uv^3, \\ \dot{v} =& -v(v + fu^2 + c_1 u^2 v + c_0 v^3), \end{aligned}$$

having the origin as a linearly zero equilibrium point.

Assuming $f = 1$ system (11) in the local chart U_2 has a common factor $v = 0$ then applying the rescaling $ds = vdt$ it is equivalent to

$$\begin{aligned} \dot{u} =& -u + auv - c_1 u^3 - c_0 uv^2, \\ \dot{v} =& -(v + u^2 + c_1 u^2 v + c_0 v^3), \end{aligned}$$

The origin of this system is a stable node. See Figure 8.

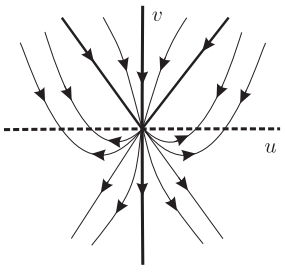

Figure 8. Local phase portrait at the origin of the local chart U_2 for system (11) when $f = 1$.

Assume now $f \in \{-1, 0\}$. In this case applying the blow up $(u, v) \to (u, w)$, where $u = u$ and $w = v/u$ and the rescaling $ds = u^2 dt$ we get the following system

$$\begin{aligned} \dot{u} =& (1-f)u - w - c_1 u^2 w + auw^2 - c_0 u^2 w^3, \\ \dot{w} =& -w(1 + aw^2), \end{aligned}$$

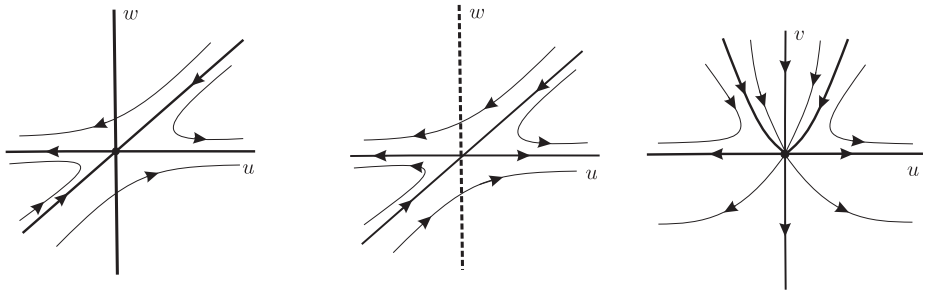

FIGURE 9. Blowing down of the origin of the local chart U_2 for system (11) when $f = -1, 0$

which has the origin as the unique singular point whose eigenvalues are -1 and $1 - f$. So this point is a saddle. From the blow down we get the local behavior of the solutions in a neighborhood of $(0, 0)$ in the local chart U_2, as shown in Figure 9.

Now we study the finite singular points. We set $\Delta = -4c_0+a(4c_1+af^2)$ and consider different cases.

Case 1: If $c_0 > 0$ and $a \geq 0$, or $c_0 > 0$, $a < 0$ and $\Delta < 0$ there are no finite singular points.

Case 2: If $c_0 < 0$, $a < 0$ and $\Delta > 0$ then we have the six finite singular points:

$$P_0^{\pm} = (0, \pm\sqrt{-c_0}),\ P_1^{\pm} = (\sqrt{-a}, (af \pm \sqrt{\Delta})/2)$$

and

$$P_2^{\pm} = (-\sqrt{-a}, (af \pm \sqrt{\Delta})/2).$$

The eigenvalues of $P_0^{\pm}$ are a and $\pm\sqrt{-c_0}$ so these points are a saddle and a stable node. The eigenvalues of $P_1^{\pm}$ are $-2a$ and $\pm\sqrt{\Delta}$ so they are an unstable node and a saddle. The eigenvalues of $P_2^{\pm}$ are $-2a$ and $\pm\sqrt{\Delta}$ so they are an unstable node and a saddle.

Case 3: If $c_0 < 0$, $a < 0$ and $\Delta = 0$ we have the four finite singular points $P_0^{\pm}$, $P_1^{+} = P_1^{-}$ and $P_2^{+} = P_2^{-}$ which are, respectively, a saddle, a stable node and two saddle–nodes.

Case 4: If $c_0 < 0$, $a < 0$ and $\Delta < 0$ then we have the two singular points $P_0^{\pm}$. P_0^{+} is a hyperbolic saddle and P_0^{-} is a stable node.

Case 5: If $c_0 < 0$ and $a > 0$ or $c_0 < 0$, $a = 0$ we have the two singular points $P_0^{\pm}$. If $c_0 < 0$ and $a > 0$ $P_0^{\pm}$ are hyperbolic points. If $c_0 < 0$, $a = 0$ the two singular points $P_0^{\pm}$ have eigenvalues $\pm 2\sqrt{-c_0}$ and 0, so they are semi–hyperbolic, applying Theorem 2.19 in [6] we get that P_0^{+} is an unstable node and P_0^{-} is a saddle.

Case 6: If $c_0 = 0$, $a < 0$ and $\Delta > 0$ we have the five singular points $P_0^{+} = P_0^{-}$, $P_1^{\pm}$ and $P_2^{\pm}$ which are, respectively, a saddle–node, an unstable node, a sadddle, an unstable node and a saddle.

Case 7: If $c_0 = 0$, $a < 0$ and $\Delta < 0$ or $c_0 = 0$ and $a > 0$ then we have the unique singular point $P_0^{+} = P_0^{-} = (0, 0)$ which is a saddle–node.

Case 8: If $c_0 = 0$, $a < 0$ and $\Delta = 0$ we have the three singular points $P_0^+ = P_0^-$, $P_1^+ = P_1^-$ and $P_2^+ = P_2^-$ and all are saddle–nodes.

Case 9: If $c_0 > 0$, $a < 0$ and $\Delta > 0$ then we have the four finite singular points: $P_1^\pm$ and $P_2^\pm$ which are, respectively, an unstable node, a saddle, an unstable node and a saddle.

Case 10: If $c_0 > 0$, $a < 0$ and $\Delta = 0$ we have the two singular points $P_1^+ = P_1^-$ and $P_2^+ = P_2^-$ which are both saddle-nodes.

Case 11: If $c_0 = 0$ and $a = 0$ then we have $P_0^+ = P_0^- = P_1^+ = P_1^- = P_2^+ = P_2^- = (0, 0)$. It is a linearly zero point. Applying the blow up $(x, y) \to (z, w)$, where $y = x/w$ and $x = x$ and the rescaling $ds = xdt$ we get the following system

$$\begin{aligned} \dot{x} = &\quad x^2 \\ \dot{w} = &\quad c_1 + (f-1)xw + w^2, \end{aligned}$$

which has the origin as a saddle point. If $c_1 > 0$ there are no singular points on $x = 0$. If $c_1 = 0$ the origin is the unique singular point. If $c_1 < 0$ then we have two finite singular points $(0, \pm 1/\sqrt{-c_1})$. They are semi-hyperbolicand applying Theorem 2.19 in [6] we get that both are saddle–nodes with $w = 0$ as an invariant line. From the blow down of the three cases we get the local behavior at the origin, given in, respectively, Figures 10.

We remark that if $a < 0$ system (11) has three invariant straight lines $x = 0$ and $x = \pm 1$. Due to the $\mathbb{Z}_2$-equivariance we can restrict the study of the global phase portrait to $x > 0$ (with the same orientation when $x < 0$).

5.1. **Global phase portraits for system** (11) **with** $f = 1$**.** The infinite is filled up of singular points. The origin of the local chart U_2 after removing the straight line of singularities remains as a singular point whose behavior is topologically equivalent to stable node, see Figure 8.

In Case 1 there are no finite singular points and so the global phase portrait is (1) of Figure 2.

In Case 2 we have six finite singular points, all of them on invariant straight lines. The α–limit of the separatrix s of the saddle P_0^+ can be P_1^+, or P_1^-, or the origin of V_2 (see Figure [**?**]). We will show that the unique possibility is P_1^+. Indeed in the other two possibilities when $c_1 \leq 0$ the vector field has at least four contact points with the straight line $y = 0$ which is not possible in view of Lemma 6. The case $c_1 > 0$ can be treated analogously choosing an straight line contact that may not be $y = 0$. This fact fixes the phase portrait for x in the strip $(-\sqrt{-a}, \sqrt{-a})$. Moreover, the α–limit of the separatrix $\bar{s}$ of the saddle P_1^- (see Figure 11 is the origin of the local chart V_2. Summing up, the unique global phase portrait is (2) of Figure 2.

In Case 3 the point P_1^+ coalesces with P_1^- and the point P_2^+ coalesces with P_2^-. Hence, by continuity from Case 2 the unique global phase portrait is (3) of Figure 2.

In Case 4 the points $P_1^\pm$ and $P_2^\pm$ become complex and since the origin of the local chart U_2 is a stable node and we have the two invariant straight lines $x = \pm\sqrt{-c}$, the unique global phase portrait in this case is (4) of Figure 2.

In Case 5 system (11) has no more $x = \pm\sqrt{-a}$ as invariant straight lines and the two singular points $P_0^\pm$ are on the invariant straight line $x = 0$. Consequently the ω–limit of the two unstable separatrix of the saddle P_0^- are either two infinite singular points of U_1 or the origin of U_2. Both possibilities hold. For the first case take $c_0 = -1$, $a = 1$ and $c_1 = -1$ or $c_0 = -1$, $a = 0$, $c_1 = 1$.

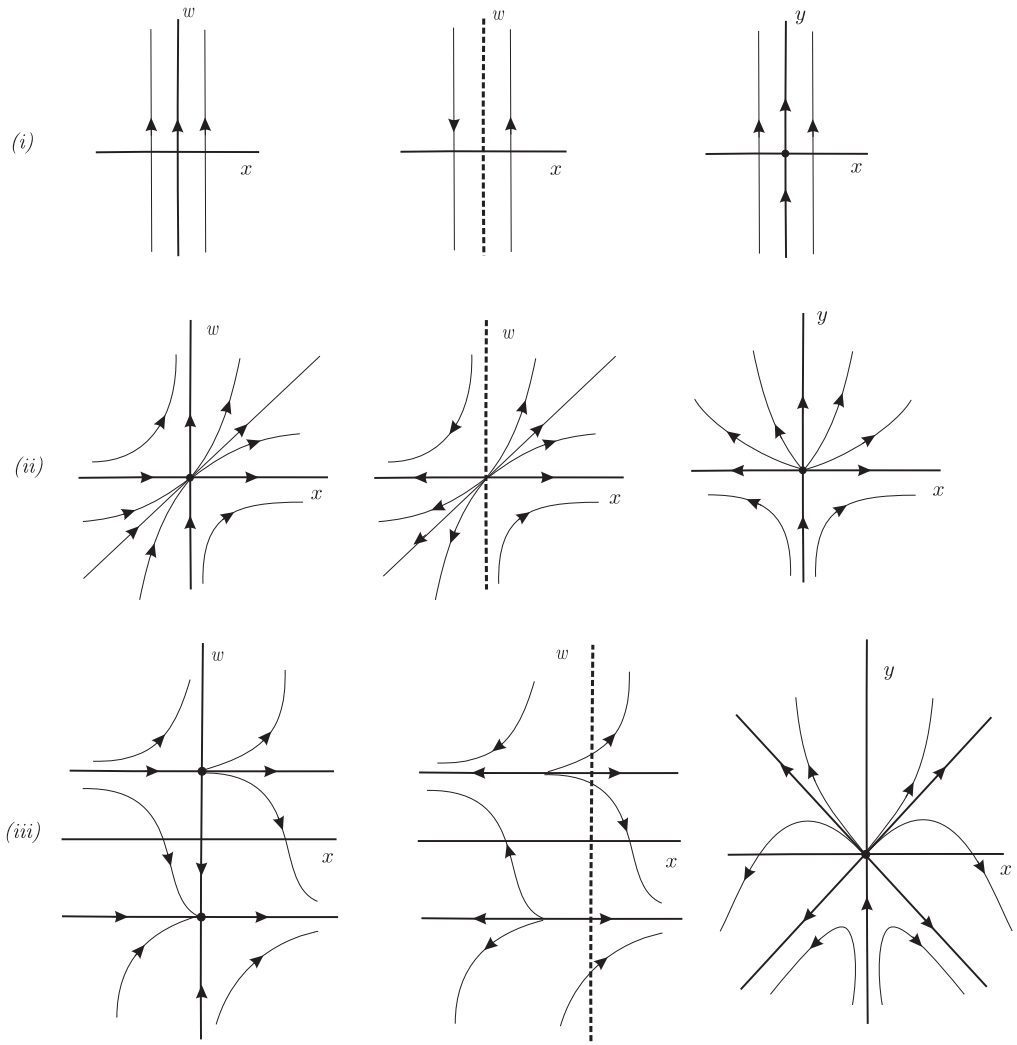

FIGURE 10. Blowing down of the origin of system (11): (i) for $c_1 \geq 0$; (ii) for $c_1 = 0$ and (iii) for $c_1 < 0$.

For the second case take $c_0 = -1$, $a = 1$ and $c_1 = 7$ or $c_0 = -1$, $a = 0$ and $c_1 = -1$. The global phase portraits are (5) and (6) of Figure 2, respectively.

Under the assumptions of Case 6 the point P_0^+ coalesces with P_0^- and by continuity from Case 2 we have the global phase portrait (7) of Figure 2.

Now we consider Case 7. When $a > 0$ and $c_0 = 0$, system (11) has no more $x = \pm\sqrt{-a}$ as invariant straight lines and the point P_0^+ coalesces with P_0^-. By continuity from Case 5 we obtain the global phase portrait given in (8) of Figure 2. When $a < 0$, $c_0 = 0$ and $\Delta < 0$ system (11) has $x = 0$ and $x = \pm\sqrt{-a}$ as invariant straight lines and the point P_0^+ coalesces with P_0^-. Again by continuity form Case 4 the global phase portrait is (9) of Figure 2.

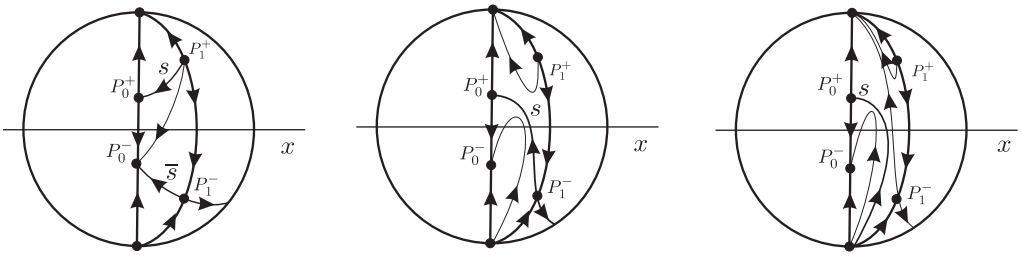

FIGURE 11. Possible α–limit of the separatrix s of the saddle point P_0^+ (see Case 2 for system (II) with $f = 1$)

For Case 8 system (11) has $x = \pm\sqrt{-a}$ and $x = 0$ as invariant straight lines and the point P_i^+ coalesces with P_i^-, for $i = 0, 1, 2$. By continuity from Case 2 we have that the unique phase portrait is (10) of Figure 2.

Under the assumptions of Case 9, the points $P_0^\pm$ are complex and system (11) has $x = \pm\sqrt{-a}$ and $x = 0$ as invariant straight lines. This case can be obtained from Case 6 when $P_0^+ = P_0^-$ tends to the origin of the local chart U_2, providing the global phase portrait (11) of Figure 2.

Consider Case 10. By continuity from Case 2 we get the phase portrait (12) of Figure 2.

Finally, in Case 11, due to the study of the local behavior of the origin, which is the unique finite singular point (see Figure 10), we have the two possible global phase portraits (8) and (13) of Figure 2, for $c_1 \leq 0$ and $c_1 > 0$ respectively.

5.2. **Global phase portrait for system** (11) **with** $f = -1$**.** We distinguish between two cases $a < 0$ and $a \geq 0$.

When $a < 0$ system (11) has $y = \pm\sqrt{-a}$ as two invariant lines and in the region limited by them the solutions behave as in the case when $a < 0$ and $f = 1$. However, in this case, the infinity is not filled up with singular points and there are only two pairs of singular points at infinity, the origin of the local charts U_1, V_1, U_2 and V_2. The origin of U_1 is a stable node and the origin of U_2 is described in Figure 9. Therefore, taking all this into account and the study made in the case $f = 1$ and $a < 0$, we conclude that in Case 1 with $c_0 > 0, a < 0, \Delta < 0$ the global phase portrait is (1) of Figure 3; in Case 2 the unique global phase portrait is (2) of Figure 3; in Case 3 the unique global phase portrait is (3) of Figure 3; in Case 4 the unique global phase portrait is (4) of Figure 3; in Case 6 the unique global phase portrait is (5) of Figure 3; in Case 7 with $c_0 = 0, a < 0, \Delta < 0$ the unique global phase portrait is (6) of Figure 3; in Case 8 the unique global phase portrait is (7) of Figure 3; in Case 9 the unique global phase portrait is (8) of Figure 3, and in Case 10 the unique global phase portrait is (9) of Figure 3.

Now we study the cases in which $a \geq 0$. These cases are: *Case 1* with $c_0 > 0$, $a \geq 0$, *Case 5* with $c_0 < 0$, $a \geq 0$, *Case 7* with $c_0 = 0$, $a > 0$ and finally *Case 11*.

In *Case 1* with $c_0 > 0$ and $a \geq 0$, there are no finite singular points and so the global phase portrait is (1) of Figure 3. In *Case 4* with $c_0 < 0$ and $a > 0$ there are two finite singular points $P_0^\pm$. Moreover, the origin of the local chart U_2 has two hyperbolic sectors. The α–limit of the stable separatrices of the origin of U_2 can be P_0^+, P_0^- or the origin of the local chart V_2. All of them are realizable. For the first case take $c_1 = 1, a = 1, c_0 = -1$ and for the third one take

$c_1 = 10, a = 1, c_0 = -1$. By continuity the second one also holds (it corresponds to a separatrix connection). Therefore we have the global phase portrait (10), (11) and (12) of Figure 3.

The *Case 7* with $c_0 = 0$ and $a > 0$ follows from *Case 5* by continuity because in this case the points P_0^+ and P_0^- coalesce. Hence we have the global phase portraits given in (13), (14) and (15) of Figure 3. Taking $c_0 = 0, a = 1$ and $c_1 = 0$ we have (13) of Figure 3 and taking $c_0 = 0, a = 1$ and $c_1 = 10$ we have (15) of Figure 3, by continuity (14) is realizable.

Under the assumption of *Case 11*, i.e., $c_0 = a = 0$ there are two possible local phase portraits at the origin according to $c_1 \leq 0$ and $c_1 > 0$ as shown in Figures 10. In the case $c_1 > 0$ there is a unique global phase portrait which is (16) of Figure 3. Taking into account that in *Case 7* we have three different realizable phase portraits one could expect that in this case, when $c_1 \leq 0$ we would also have the three phase portraits (13), (14) and (15) of Figure 3. However, since

$$\dot{y}|_{y=0} \leq 0 \quad \text{when} \quad c_1 \leq 00$$

we conclude that only phase portrait (13) in Figure 3 holds.

5.3. **Global phase portrait for system** (11) **with** $f = 0$ **and** $a = 1$**.** We already showed that the local phase portraits at the infinite singlar points of system (11) in the local charts U_1 and U_2 behave in the same way when $f = 0$ or $f = -1$. Moreover, when $a = 1$ the finite singular points depend on $c_0 < 0, c_0 = 0, c_0 > 0$. In all these three cases the finite singular points when $f = 0$ and when $f = -1$ are the same. We recall that since $a = 1$ we only have $x = 0$ as an invariant straight line. Taking all this into account and the study done in subsection 5.2 with $a > 0$, we conclude that: when $c_0 > 0$ the unique possible phase portrait is (1) of Figure 3; when $c_0 = 0$ taking $a = 1$ and $c_1 = 0$ we get the phase portrait (13) of Figure 3 and taking $a = 1$ and $c_1 = 10$ we get the phase portrait (15) of Figure 3, by continuity the phase portrait (14) of Figure 3 is also realizable. Moreover when $c_0 < 0$ the possible phase portraits are (10), (11) and (12) of Figure 3. (10) is realizable for $a = 1, c_0 = -1$ and $c_1 = 3$ and (12) is realizable for $a = 1, c_0 = -1$ and $c_1 = 12$ then (11) is holds by continuity.

5.4. **Global phase portrait for system** (11) **with** $f = 0$ **and** $a = -1$**.** The study of the local phase portraits of the finite and infinite singular points follows from the case $f = -1$ and $a = -1$ (see subsection 5.2). However when $c_0 = 0$, $a = -1$ and $\Delta = 0$ (see *Case 8*) we get that $c_1 = 0$ and so $y = 0$ becomes an invariant straight line (this does not happen in subsection 5.2). So, in this particular case, we get a new global phase portrait which is (17) of Figure 3. All the rest follow from the arguments given in subsection 5.2 with $a = -1$. They are (1) of Figure 3 for *Case 1*; (2) of Figure 3 for *Case 2*; (3) of Figure 3 for *Case 3*; (4) of Figure 3 for *Case 4*; (5) of Figure 3 for *Case 6*; (6) of Figure 3 for *Case 7*; (8) of Figure 3 for *Case 9*, and (9) of Figure 3 for *Case 10*.

6. Global behavior of systems (V) and (VI) of Theorem 2

Now we study of the local phase portraits of the finite and infinite singular points of systems (V) and (VI) of Theorem 2. Note that systems (V)- (VI) can be written as the following system

$$\begin{aligned} \dot{x} &= x, \\ \dot{y} &= c_0 + c_1 x^2 + y^2 + f x^2 y, \end{aligned} \tag{12}$$

with $f \in \{-1, 1\}$ and $c_0, c_1 \in \mathbb{R}$.

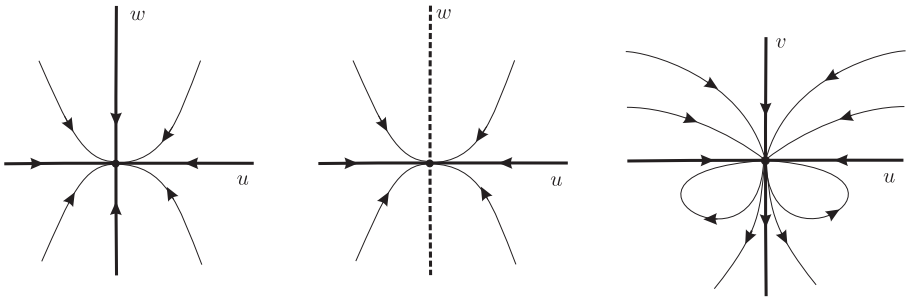

FIGURE 12. Blowing down of the origin of the local chart U_2 for system (V)

When $c_0 > 0$ system (12) has no finite singular points. When $c_0 < 0$ it has the two singular points P_0^+ which is an unstable node and P_0^- which is a saddle. If $c_0 = 0$ then $P_0^+ = P_0^-$ and it is a saddle-node.

The Poincaré compactification $p(\mathcal{X})$ of system (12) in the local chart U_1 is given by

$$\begin{aligned} \dot{u} &= fu + c_1 v + u^2 v - uv^2 + c_0 v^3, \\ \dot{v} &= -v^3. \end{aligned} \tag{13}$$

There is a unique singular point in the local chart U_1 which is the origin. It is semi-hyperbolic because the eigenvalues are 0 and f. Using Theorem 2.19 of [6] we conclude that if $f = -1$ the origin is topologically equivalent to a stable node, and if $f = 1$ the origin is topologically equivalent to a saddle.

System (12) in the local chart U_2 is written as

$$\begin{aligned} \dot{u} &= -uv - fu^3 + uv^2 - c_1 u^3 v - c_0 uv^3, \\ \dot{v} &= -v(v + fu^2 + c_1 u^2 v + c_0 v^3). \end{aligned}$$

It has the origin as a linearly zero equilibrium point.

Applying the blow up $(u, v) \to (u, w)$, where $u = u$ and $w = v/u$ and the rescaling $ds = u^2 dt$ we get the following system

$$\begin{aligned} \dot{u} &= -fu - w - c_1 u^2 w + uw^2 - c_0 u^2 w^3, \\ \dot{w} &= -w^3, \end{aligned}$$

which has the origin as a singular point when $u = 0$. This is a semi hyperbolic point and again, applying Theorem 2.19 of [6], we get that when $f = 1$ this point is topologically equivalent to a stable node and when $f = -1$ this point is topologically equivalent to a saddle. From the blow down we get that the local behavior of the solutions in a neighborhood of the origin in the local chart U_2, are the ones given, respectively, in Figure 9 when $f = -1$ and in Figure 12 when $f = 1$.

6.1. **Global phase portrait for system** (12) **with** $f = -1$**.** The local phase portraits of the finite and infinite singular points of system (12) when $f = -1$ are the same as in subsection 5.2 when $a \geq 0$. Hence the global phase portraits are (1) of Figure 3 when $c_0 > 0$; (13), (14) and (15) of Figure 3 when $c_0 = 0$, and (10), (11) and (12) of Figure 3 when $c_0 < 0$. Indeed, we get (13) if $c_0 = 0, a = 1, c_1 = 0$ and (15) if $c_0 = 0, a = 1, c_1 = 10$, by continuity (14) is realizable and, we get (10) if $c_0 = -1, a = 0, c_1 = 3$ and (12) if $c_0 = -1, a = 0, c_1 = 12$ then, by continuity (11) is realizable.

6.2. **Global phase portrait for system** (12) **with** $f = 1$**.** When $c_0 < 0$ there are two finite singular points $P_0^{\pm}$ which are an unstable node and a saddle. The origin of the local chart U_1 is a saddle and the local behaviour of the origin of the local chart U_2 is the one given in Figure 12. So, we have three possible global phase portraits depending on of the α-limit of the stable separatrices of the saddle in the origin of the local chart U_1 is P_0^+, P_0^- or of the origin of the local chart V_2. All possibilities hold and we get, respectively, the global phase portraits (1), (2) and (3) of Figure **??**. The phase portrait (1) is realized when $c_1 = 1$, $c_0 = -2$; the phase portrait (3) is realized when $c_1 = 10$, $c_2 = -2$, and by continuity, the phase portrait (2) also holds (note that it corresponds to a separatrix connection).

When $c_0 = 0$ the two finite singular points coalesce to a unique point which is a saddle-node. The infinite behaves as described above. By continuity we have also three possible global phase portraits that are realized. They are (4), (5) and (6) of Figure 4. For the phase portrait (4) take, for instance $c_1 = -1$; for the phase portrait (5) take $c_1 = 0$ and for the phase portrait (6) take, for instance, $c_1 = 1$.

Finally, when $c_0 > 0$ there are no finite singular points. This fact together with the study of the infinity done above, imply that there is a unique possible global phase portrait which is (7) of Figure 4.

Acknowledgements

The first author is partially supported by MINECO grants MTM2016-77278-P and MTM2013-40998-P, an AGAUR grant number 2014SGR-568, the grant FP7-PEOPLE-2012-IRSES 318999. The first two authors are partially supported by CAPES grant number 88881.030454/2013-01 from the program CSF-PVE. The second author is partially supported by FAPESP grant "Projeto Temático" 2014/00304-2. The third author is partially supported by FCT/Portugal through UID/MAT/04459/2013.

This paper was partially developed during the visit of the third author to ICMC-USP supported by the project APV-CNPq number 450511/2016-2

References

[1] H. Aminikhah and M.Hemmatnezhad, *An efficient method for quadratic Riccati differential equation.* Commun. Nonlinear Sci. Numer. Simul. **15** (2010), 835–839.

[2] B.D.O. Anderson and J. B. Moore, *Linear Optimal Control.* Prentice Hall, 1971.

[3] B.D.O. Anderson and J.B. Moore, *Optimal Filtering*, Prentice-Hall, Englewood Cliffs, NJ, USA, 1979.

[4] S. Bittanti, P. Colaneri and G. De Nicolao, *The periodic Riccati equation in the Riccati equation*, Communications and Control Engineering, Springer, Berlin, Germany (1991), 127–162.

[5] S. Bittanti , P. Colaneri and G.O. Guardabassi, *Periodic solutions of periodic Riccati equations*, IEEE Trans. Autom. Control **29** (1984), 665–667 .

[6] F. Dumortier, J. Llibre and J. C. Artés, *Qualitative Theory of Planar Differential Systems*, UniversiText, Springer-verlag, New York, 2006.
[7] G.A. Einicke , L.B. White and R.R. Bitmead, *The use of fake algebraic Riccati equations for co-channel demodulation*, IEEE Trans. Signal Process. **51** (2003), 2288–2293.
[8] M. Gerber, B. Hasselblatt and D. Keesing, *The Riccati equation: pinching of forcing and solutions*, Exp. Math. **12** (2003) 129–134.
[9] R.E. Kaiman, *New methods in Wiener filtering. Proc. of First Symp. on Eng. Applications of Random Function Theory and Probability* (J. Bogdanoff and F. Kozin eds.), J. Wiley 1963, 270–388.
[10] R.E. Kalman, Y.C. Ho and K.S. Narendra, *Controllability of linear dynamical systems*, Contrib. Differ. Equ. **1** (1963), 189–213.
[11] H. Kwakernaak and R. Sivan, *Linear Optimal Control Systems*. J. Wiley, 1972.
[12] J.S.W. Lamb and M. Roberts, *Reversible equivariant linear systems*, J. Differential Equations **159** (1999), 239–279.
[13] J. Llibre, B.D. Lopes and P.R. da Silva, *Phase portraits of Riccati quadratic polynomial differential systems*, preprint, 2016.
[14] F. Mohammadi and M. M. Hosseini, *A comparative study of numerical methods for solving quadratic Riccati differential equations*. J. Franklin Inst. **348** (2011), 156–164.
[15] D. Neumann, *Classification of continuous flows on 2-manifolds*, Proc. Amer. Math. Soc. **48** (1975), 73-81.
[16] J. F. Riccati, *Animadversiones in aequationes differentiales secundi gradus*. Acta Eruditorum Lipsiae, Supplementa, VIII, II (1724), 66–73.
[17] W.T. Reid, *Riccati Differential Equations, Mathematics in Science and Engineering* **86**, Academic Press, New York, NY, USA, 1972.

[1] Departament de Matemátiques, Universitat Autònoma de Barcelona, 08193 Bellaterra, Barcelona, Catalonia, Spain
E-mail address: jllibre@mat.uab.cat

[2] Departamento de Matemática, ICMC-Universidade de São Paulo, Avenida Trabalhador São-carlense, 400 - 13566-590, São Carlos, SP, Brazil
E-mail address: regilene@icmc.usp.br

[3] Departamento de Matemática, Instituto Superior Técnico, Universidade Técnica de Lisboa, Av. Rovisco Pais 1049–001, Lisboa, Portugal
E-mail address: cvalls@math.ist.utl.pt